Submodule Integrated Distributed Maximum Power Point Tracking for Solar Photovoltaic Applications

Robert C. N. Pilawa-Podgurski, *Member, IEEE*, and David J. Perreault, *Senior Member, IEEE*

***Abstract*—This paper explores the benefits of distributed power electronics in solar photovoltaic applications through the use of submodule integrated maximum power point trackers (MPPT). We propose a system architecture that provides a substantial increase in captured energy during partial shading conditions, while at the same time enabling significant overall cost reductions. This is achieved through direct integration of miniature MPPT power converters into existing junction boxes. We describe the design and implementation of a high-efficiency (>98%) synchronous buck MPPT converter, along with digital control techniques that ensure both local and global maximum power extraction. Through detailed experimental measurements under real-world conditions, we verify the increase in energy capture and quantify the benefits of the architecture.**

***Index Terms*—DC-DC power converters, energy harvesting, photovoltaic cells, power integrated circuits, solar energy.**

I. Introduction

With rising world-wide energy demands and soaring prices of fossil fuels, interest in renewable energy sources has increased. Among these, solar photovoltaic (PV) energy has seen a rapid growth in the last few years, resulting in decreased prices of PV panels as production capacity increases at a fast pace. As the PV panel prices decrease, the cost of the power electronics required to extract the maximum power of the PV panels and to interface the PV system to the grid is becoming a larger part of the overall system cost [1]. Much attention has, therefore, been given to the development of power electronics that enable a cost reduction of the overall system. In addition, much research is focused on increasing the efficiency of the power processing stage, as well as on improving the power yield of the overall system [2], [3].

Many PV installations suffer from current mismatch between different panels, due to nonuniform shading of the array, dirt accumulation, or manufacturing variability. Ensuring uniform illumination is particularly challenging in residential PV applications, where large current mismatch can be present due to external objects that cause shading. Shown in Fig. 1(a) is the most common solar PV architecture, which connects all panels in series. In this architecture, any partial shading or other source of cell current mismatch will cause the overall system output power to be reduced, since the current in the string is limited by the weakest panel. While panels used today typically employ bypass diodes that help protect the panels and limit the negative effect of partial shading, it is still the case that partial shading has a significant negative effect on any solar installation.

The microinverter (also known as panel-level inverter or ac-module) concept shown in Fig. 1(b) has been exploited to address this problem by operating each panel at its unique maximum power point (MPP), and providing separate dc-to-ac conversion for each panel. Using this architecture, any shading of a single panel only affects its output power, without limiting the performance of the other panels in the installation. While the microinverter architecture can increase overall energy capture in a system, microinverters typically suffer from lower overall efficiency than high-voltage string-level inverters, owing to the large voltage transformation required to interface the panel voltage (e.g., 20–40 V_{DC}) to the grid (e.g., 120–240 V_{AC} rms), and often suffer from relatively high cost.

Recently, the concept of cascaded dc-dc converters (dc–dc optimizers) has become popular [4]–[6], where each PV panel employs a dc–dc converter that performs maximum power point tracking (MPPT), and the outputs of the converters are connected in series. This architecture is shown in Fig. 1(c). Through dc–dc optimizers, localized control of panel voltage and current can be achieved, and each panel can operate at its independent MPP, thus improving the energy extraction of the overall system. The series connection of the outputs provides an inherent voltage stacking that enables each dc–dc converter to operate at a relatively low-voltage conversion ratio (enabling high conversion efficiency), while still achieving high overall output voltage, which is desirable as it enables the use of a central, high-voltage, high-efficiency inverter.

To date, however, the promise of dc–dc optimizers has not been fully realized, primarily due to the difficulty of simultaneously achieving high conversion efficiency *and* low cost of the power electronics. Low dc–dc conversion efficiency can easily negate any increase in energy capture that is offered by more localized (panel-level) control and must therefore be addressed. It should be mentioned that it is not merely the efficiency of the power electronics that must be addressed, but also how much of the available power that is extracted. It is possible to employ circuit architectures that achieve very high power conversion efficiency, such as switched-capacitor converters [7], but which does not achieve maximum power extraction, due to an inability to operate over a wide voltage range. A goal is thus to achieve

Manuscript received May 15, 2012; revised July 12, 2012; accepted September 7, 2012. Date of current version December 7, 2012. This work was supported by the National Science Foundation under Grant 0925147. Recommended for publication by Associate Editor T. Suntio.

R. C. N. Pilawa-Podgurski is with the University of Illinois at Urbana-Champaign, Urbana, IL 61801 USA (e-mail: pilawa@illinois.edu).

D. J. Perreault is with the Research Laboratory of Electronics, Massachusetts Institute of Technology, Cambridge, MA 02139 USA (e-mail: djperrea@mit.edu).

Color versions of one or more of the figures in this paper are available online at http://ieeexplore.ieee.org.

Digital Object Identifier 10.1109/TPEL.2012.2220861

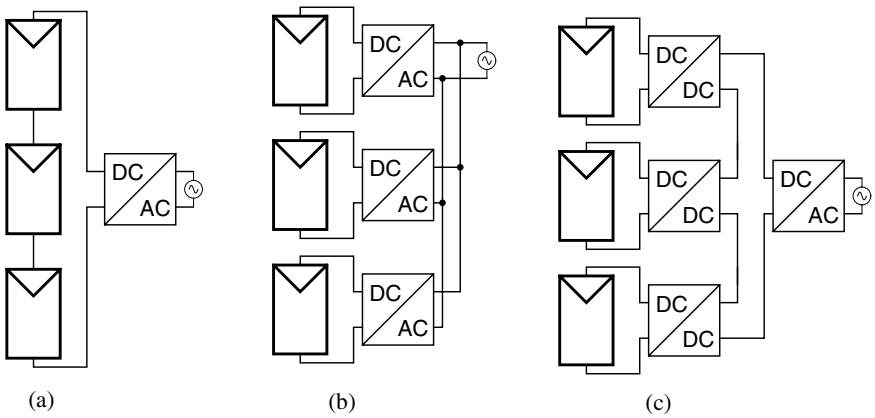

Fig. 1. Schematic drawings of three kinds of distributed MPPT architectures for solar PV. (a) Series string architecture. (b) Microinverter architecture. (c) Cascaded dc–dc (dc–dc optimizer) architecture.

very high conversion efficiency in the power electronics, *as well as* high tracking efficiency (a measure of how close to the true MPP the panel is operated).

Furthermore, a solution that increases total energy capture by a few percent, but which also increases the overall cost by more than the monetary value of the increased power (as compared to the installed system cost), will likely fail in the marketplace. In this paper, we present a dc–dc optimizer system that achieves both low cost and high conversion efficiency, while at the same time capturing substantially *more* energy than dc–dc optimizer architectures presented to date. In addition, detailed field experiments are presented that illustrate the benefits of our architecture under real-world partial shading conditions.

This paper is organized as follows. Our proposed system is presented in Section II, and Section III provides implementation details of the power converter designed for our architecture. The control implementation is discussed in Section IV, and experimental results and analysis are provided in Section V. A quantitative comparison to previous work is presented in Section VI, where we also introduce a figure of merit (FOM) that incorporates cost, efficiency, and increase in energy capture. Finally, Section VII concludes this paper.

II. Proposed Architecture

DC–DC optimizer systems can be implemented with several different circuit topologies. Previous work at the panel level has employed boost converters [5], [8] and noninverting buck–boost converters [6]. While boost converters are an attractive option because of their ability to increase the output voltage (requiring fewer panels for a given desired output voltage), their chief disadvantage is their limited operating range. As discussed in [5] and [9], since the output current of a boost converter can never be higher than its input current, the range over which current mismatch can be addressed is severely limited. The noninverting buck–boost converter is employed in [6] and can provide an output current that is both higher and lower than the input current, thus providing both a voltage increase and the ability to handle shaded panels (although within a limited range, since each converter only operates in buck or boost mode at a given time). The chief disadvantages of the noninverting buck–boost topology are the increased number of transistors, and the achievable conversion efficiency, which is typically lower than buck or boost converters for the same switch rating. A more detailed performance analysis of a number of potential power converter topologies for dc–dc optimizers can be found in [10].

In this paper, we chose to implement the dc–dc optimizer system using synchronous buck converters. While the synchronous buck topology enables both high switching frequency (important for small size, low cost) and high efficiency, it does not contribute any voltage gain (which would reduce the number of panels that must be series connected). In most residential and utility-based installations, however, there are a sufficient number of PV panels to provide for the inherent stacking of voltages without requiring the additional step-up from the power converter. When not tasked with providing additional voltage step-up, the power stage can be optimized for size, cost, and efficiency. As our experimental results indicate, the synchronous buck converter topology offers size, cost, and efficiency benefits, and the system can be operated in a manner where the control implementation is relatively simple. Meanwhile, the string current can be kept sufficiently low so that the added wiring conduction losses are kept to a minimum. In addition, as will be discussed in the experimental section, cascaded buck converter systems can often-times produce an output voltage that is *higher* than a conventional system under partial shading condition.

In order to increase the overall system energy capture, our design employs submodule distributed MPPTs, as shown in Fig. 2.[1] Using this architecture, mismatch between different submodules within the same panel can be mitigated, which yields an increase in energy capture compared to panel-level MPPTs. Furthermore, each MPPT in Fig. 2 only sees a third of the panel voltage and can thus be designed using components with lower voltage rating than panel-level MPPTs. The use of low-voltage power MOSFETs with their small parasitics in turn enables an increase in achievable switching frequency, which enables reduced passive component size and cost. As will be shown in Section III, it is even possible to miniaturize the MPPTs to the

[1]We will refer to all cells in a PV panel that are connected to the same bypass diode as a submodule. The most common type of PV panels comprise three submodules.

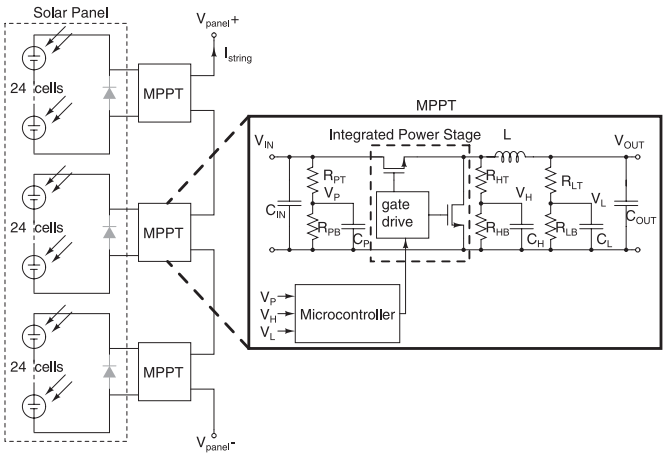

Fig. 2. Schematic drawing of the submodule integrated MPPT system. A component listing is provided in Table I.

point where they can fit in the existing standard junction box at the back of the PV panel. This leads to further cost reductions, as a large custom outdoor-rated enclosure contributes significant cost to a dc–dc optimizer system.

III. Submodule Distributed MPPT Converter

The inset of Fig. 2 shows a schematic drawing of the submodule MPPT architecture designed as part of this study. The system comprises a synchronous buck converter power stage controlled by a microcontroller to achieve local MPP operation. The microcontroller can sense voltage and also employs lossless current sensing [11] for control algorithms that also require current information. The input voltage is sensed (node V_P) through the attenuating low-pass filter comprising R_{PT}, R_{PB}, and C_P. Likewise, the output voltage is sensed (node V_L) through the attenuating low-pass filter comprising R_{LT}, R_{LB}, and C_L. With the addition of the attenuating low-pass filter comprising R_{HT}, R_{HB}, and C_H, the average voltage across the inductor ($V_H - V_L$) can be measured, which gives a signal that is proportional to the inductor current. Note that the inductor current was not needed in the control algorithms that we employed in this study, but was recorded in this manner for diagnostic purposes.

Each converter employs an isolated I2C communication interface, enabling bidirectional information transfer to a master node, which can be a dedicated microcontroller or a computer. It should be noted that each MPPT can operate without any communication interface, but the I2C interface is used here to gather diagnostic data from each converter, and to provide a simple means for controlling the global output power. Table I provides a listing of the components used in the design. A complete bill-of-material and cost analysis can be found in [10].

Shown in Fig. 3(a) is a photograph of the complete converter prototype, together with a pencil for scale; the overall converter "box volume" is 4 cm^3 . Shown in Fig. 3(b) is one of the MPPTs placed in a typical solar panel junction box. In a full installation, three converters are used per PV panel, one in parallel with each bypass diode. It is evident from the photograph that

TABLE I
Component Listing

Device	Model	Value	Manufacturer
Integrated Power Stage	FDMF6704A		Fairchild
L	SER1360-103KL	10 μH	Coilcraft
R_{HT}, R_{LT}, R_{PT}	0402	100kΩ	Panasonic
R_{HB}, R_{LB}, R_{PB}	0402	10kΩ	Panasonic
C_H, C_L, C_P	0402	1 μF	Murata
C_{IN}	1206, X5R, 25V	3 x 10 μF	Murata
C_{OUT}	1206, X5R, 25V	2 x 10 μF	Murata
Microcontroller	ATtiny861		Atmel

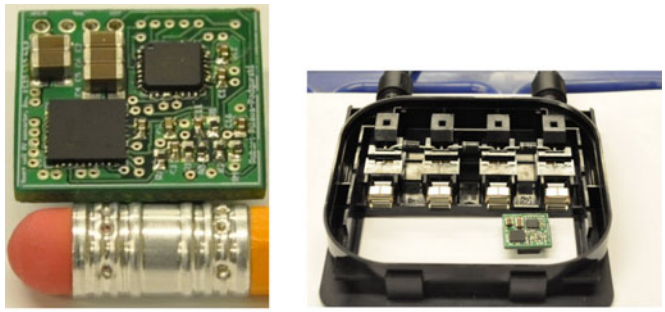

Fig. 3. Photographs of submodule MPPT hardware. (a) Photograph of the submodule MPPT converter, with a pencil shown for scale. The power inductor is on the bottom side of the PCB. (b) Photograph showing the submodule MPPT together with a solar panel junction box. The three bypass diodes are also visible; an MPPT converter is placed in parallel with each diode.

TABLE II
Converter Specifications

Input Voltage Range	5-27 V
Output Voltage Range	0.8-20
Max Output Power	80 W
Switching Frequency	250 kHz
Converter Peak Efficiency	98.2%

three converters fit in the junction box, with plenty of space for connectors and sufficient air flow for passive cooling. A goal of the power stage design was to achieve a small enough converter footprint to fit into the junction box on the back of off-the-shelf PV panels. By utilizing the existing weather-resistant junction box as an enclosure, significant cost savings can be realized. The integrated power stage is a combined gate drive and power MOSFET chip (FDMF6704A), which also incorporates a 5-V linear regulator, enabling the converter to be completely powered from the submodule.

In order for the submodule distributed MPPT architecture of Fig. 2 to be effective, it is important that the additional power captured is not wasted by low conversion efficiency of the power electronics. Much care was thus taken in this study to achieve high-efficiency operation, both through the choice of topology and passive components, as well as the implementation of sensing and control. A detailed description of these efforts can be found in [10]. Shown in Table II is an overview of the specifications of the converter, along with a performance summary.

A detailed efficiency and power characterization of the MPPT converter has been carried out to measure performance across

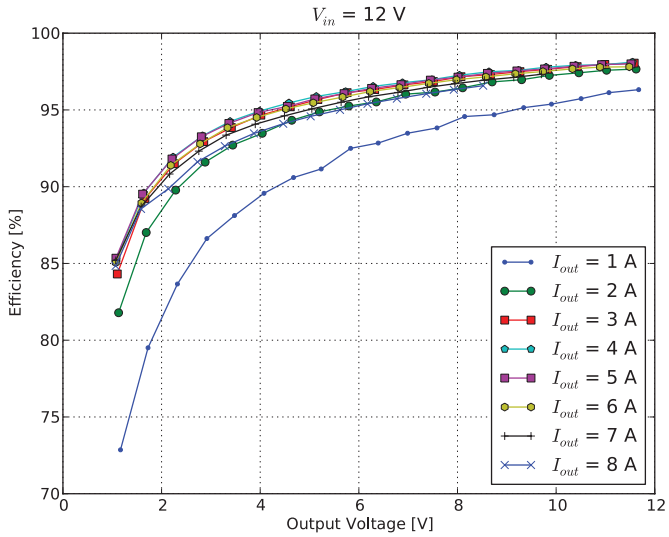

Fig. 4. Measured efficiency versus output voltage, parameterized by output current. A lower output voltage corresponds to a shaded submodule, while a lower output current signifies a string with less insolation.

a wide load and output voltage range. Fig. 4 shows a plot of efficiency versus output voltage, parameterized by output current, for a fixed input voltage of 12 V. No attempts were made in this design to provide increased light-load efficiency, but we note that in general, this can be accomplished with suitable light-load control scheme, such as pulse-frequency modulation, if desired. The converter will operate at lower output voltages if it suffers from more shading relative to the other converters in the string. A low output current would signify that the insolation of the entire string of MPPTs is relatively low.

Given these characteristics of the system, it is important to achieve high efficiency at high power levels (for maximum total energy capture), as well as at operating points where the converter is expected to spend significant time in real-world scenarios. In Fig. 4, this would correspond to high output voltage (no or little shading) and high current (>5 A, corresponding to high insolation). We see from the plot that we achieve an efficiency above 97% under these conditions. The peak efficiency of 98.2% is realized at an input voltage of 16 V and an output current of 5 A. It should be noted that all efficiency measurements include all sensing, gate drive, and control losses, as the converter itself is powered from its input terminals. A more detailed performance characterization of the power stage across a variety of operating conditions can be found in [10]; excellent efficiency is maintained across an input range from 8 to 16 V, and the converter functions over a still much wider range.

IV. Control Implementation

In conventional solar PV installations, the inverter must control the voltage (or current) of the string of PV modules to ensure that the system is operating at the MPP. An additional challenge in situations with partial shading is the fact that when the bypass diodes conduct around weak modules, the resulting I–V characteristics of the overall system can contain several maxima, of which typically only one is a true global maximum. Most inverters periodically sweep the output voltage of the PV array to detect such situations and to ensure that the system operates at the true global MPP. Distributed MPPT (DMPPT) systems present additional challenges, and complicated models have been used to simulate their behavior [12]. In this study, we seek to implement a control method that extracts maximum energy from the DMPPT system, while keeping the overall complexity to a minimum.

In our architecture, owing to the subpanel integrated dc–dc converters, there are no local maxima in the I–V characteristics of the overall system, as each submodule provides whatever voltage it can to the system, while all submodules share the same output current. In order to extract maximum energy from a PV installation with submodule power tracking, each MPPT must continuously operate its submodule at the correct current and voltage, while also allowing all other MPPTs do the same for their individual submodules. We must thus design a control algorithm that ensures that each submodule operates at its *local* MPP, while also ensuring that the overall system operates at the *global* MPP (i.e., the overall string voltage and current are such that all submodules are operating at their respective MPPs).

A. Local MPPT Algorithm

Since the outputs of the individual power trackers are connected in series (as seen in Fig. 2), all of them share the same output current I_{string}. If the number of series-connected converters is large (which is typically the case in a system installation, where a large output voltage is desired), the string current (from the perspective of a single MPPT) can be considered constant. With a constant output current, each converter can then maximize its own output power by maximizing its output voltage. It thus follows that a local MPPT algorithm can be implemented by driving the local output voltage to its maximum value. We can denote the output voltage of the ith converter $V_{\text{out},i}$, and the output voltage of the string of PV modules V_{string}. The output current of the string of PV modules, I_{string}, is the same as the output current of each local converter, since they are series-connected. The local control objective thus becomes

$$\arg \max_{D_i \in \langle 0,1 \rangle} \left(V_{\text{out},i}(D_i) \times I_{\text{string}} \right) \tag{1}$$

where each converter strives to find the duty cycle D_i which will maximize the output power.

In our implementation, we employ a perturb and observe (P&O) algorithm that continuously tracks the MPP by making small changes to the duty cycle in order to drive the converter output voltage to its maximum. Shown in Fig. 5 is a flowchart diagram of the local MPPT algorithm.

In order to quickly locate the approximate location of the MPP, the converter starts by performing a coarse sweep of its duty cycle and measuring the corresponding values of output voltage. The duty cycle corresponding to the maximum voltage observed is recorded, and at the end of the startup sweep, the converter is set to operate at this duty cycle. At this point, the steady-state tracking algorithm begins, which uses a P&O algorithm which aims to maximize the converter output voltage by making small changes (ΔD) to the duty cycle D. In this

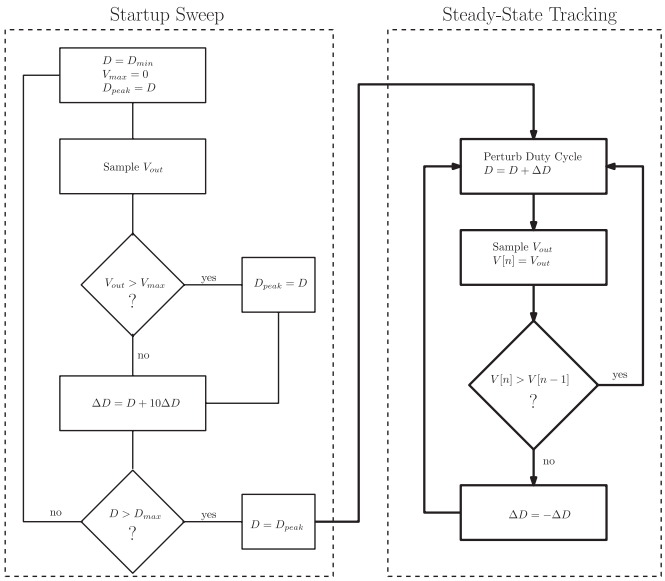

Fig. 5. Flowchart diagram illustrating the local MPPT algorithm. The approximate MPP is first found via a coarse startup sweep, followed by a P&O algorithm that strives to maximize converter output voltage.

TABLE III
MPPT TRACKING PARAMETERS

MPPT Duty Cycle Step-Size	0.8%
MPPT Startup Sweep Step-Size	5%
Minimum Duty Cycle	10%
Maximum Duty Cycle	99 %
ADC Resolution	10 bit
ADC Samples Per Measurement (Oversampling)	100

manner, the submodule MPPT will continuously track the MPP and oscillate around it to within the finite precision of its voltage sensing and duty cycle control.

The MPPT P&O rate used in our experiments was 10 Hz. It should be pointed out that this rate was limited by the I2C communication bandwidth. The delay between each time step was caused by each converter communicating its input and output voltage, as well as duty cycle to the computer for data analysis. The microcontroller itself is capable or operating at an MPPT rate in excess of 25 kHz, which is significantly faster than what is required for this application. Table III provides information about our sensing and pulsewidth modulation (PWM) resolution and step-size for the experimental prototype. The minimum achievable duty cycle step-size with the hardware we implemented was 0.4%, but the 0.8% step-size provided a good tradeoff between conversion speed and steady-state accuracy. The minimum achievable duty cycle step-size is governed by the ratio of our switching frequency (250 kHz) and the frequency of the phase-locked loop that drives the PWM components of our microcontroller (64 MHz).

B. Global MPPT Algorithm

The local MPPT algorithm that we have implemented has the attractive feature of not requiring any local current sensing, which would add both cost, complexity, and power loss to the overall solution. In order to ensure that the overall system operates at the MPP, the central controller (typically an inverter) must adjust the string current I_{string}. Previous work on global control in DMPPT applications has relied on *time synchronization* between the inverter and the local converters [13], [14]. In [13], a circuit topology (the "two-stage chopper") is employed where each converter operates for only a brief period of time, and the switching of each converter is updated sequentially. In this approach, each local converter is directly controlled by the central converter, as it controls each switching transition. In addition to poor utilization of the power converters in this approach, the control method does not scale well to large numbers of converters, as the control complexity grows quickly and the tracking speed decreases linearly with the number of converters. The control method of [14] is similar to that of [13], but here regular boost converters are employed as local converter. Each converter is sequentially perturbed in a P&O approach, and the global output power is measured to guide the direction of the next perturbation. Similarly to [13], the achievable tracking speed of the system decreases linearly with N, and the central inverter must be able to communicate with each local converter. Both of these approaches rely on time synchronization between the central inverter and the local converters.

The control method employed in this study does not require time synchronization, but rather relies on *frequency separation* to achieve improvements in achievable tracking speed and possible reduction in communication hardware. By adjusting the duty ratio, the local MPPT can autonomously achieve MPP operation so long as the submodule current at its MPP is equal to or less than that of the string.[2] To achieve global MPP operation, each submodule controller adjusts its duty ratio for MPP operation (e.g., in a "fast" loop) based on the string current, while the system level controller (typically implemented by the grid-interface inverter) adjusts the string current (in a "slow" loop) such that there is just sufficient string current available for the submodule with the highest MPP current. In this manner, the control problem can be separated into a local MPPT control for each submodule, along with a single global control loop that only requires limited information.

A key requirement for our control method to work is that there is sufficient time between changes in the string current for the local converters to reach their new local MPP equilibrium, so that the change in power can be observed by the central controller. Practically, the local MPPT frequency in our implementation has an upper bound of approximately 25 kHz (with a switching frequency of 250 kHz). We estimate that the central MPPT frequency in this scenario should be below 2.5 kHz (ten times slower). In practice, much lower central MPPT frequencies are typically employed, owing to the low switching frequency of the high-voltage, high-power electronics, and the relatively slow changes in insolation that the system is experiencing. For a system with N local converters, the central converter thus must

[2]This constraint is due to the chosen power converter topology (buck converter), which can only provide an output current greater than or equal to the input current.

strive to maximize the total output power, given by

$$\sum_{i=1}^{N} V_i(I_{\text{string}}, D_i) \times I_{\text{string}} \tag{2}$$

where we have denoted the local converter output voltage by $V_i(I_{\text{string}}, D_i)$ to make explicit its dependence on the string current (the global control variable) *and* D_i (the local control variable).

1) One-bit Feedback Global Algorithm: One method to ensure that the overall system is operating at the global MPP is to signal to the global ("slow") loop controller when one of the local MPPTs is operating at or near its maximum permitted duty cycle. At this point, the system loop controller may not decrease the current I_{string} any further, as the strongest MPPT would then not be operating at its MPP. This 1-bit feedback signal can be implemented either using a very simple single-interconnect or zero-interconnect communications link, or by encoding the information to communicate it directly via the series string interconnect. (We note that such methods are well known in other types of distributed power conversion systems [15], [16] and can be implemented without significant expense in this application.) One disadvantage of this method is that it would require the global controller (the inverter in a typical installation) to implement this functionality, such that separate dedicated hardware and firmware is required at the inverter level. This is similar to the limitations of [13] and [14], both of which also require dedicated communication hardware between the local converters and the central inverter. A benefit of the approach presented here is that the control method scales well with the number of local converters N, since each local converter operates independently of the central inverter and only communicates with the central inverter when the string current is too low (and typically only the strongest of the local converters communicates this information).

2) Communicationless Global Algorithm: It is also conceivable that with the appropriate submodule level control, global MPP operation can be ensured without *any* communication between individual converters, or between converters and the string-level inverter. All PV inverters used with conventional solar panels today already implement an MPPT functionality. It would be highly desirable to leverage this existing infrastructure to achieve both global and local optimization with existing inverter hardware.

If the global MPPT controller draws too little current, the strongest MPP will operate at its maximum duty cycle, and its submodule will deliver I_{string}, which will be less than its I_{mpp}. Since this submodule is no longer operating at its individual MPP, the overall output power of the string will decrease. When the global controller detects this decrease in power, it will act to reverse this change, thus increasing the string current. The global MPPT algorithm itself can thus ensure that the string current is not operating at a current that is lower than the highest I_{mpp} of the submodules.

The buck topology can theoretically produce any output current that is higher than its input current (although there are certainly practical limits such as device parasitics, duty cycle resolution, and loss mechanisms that limit the maximum output current). In a real converter, the conduction losses in the MOSFETs, inductor, and wiring will increase as the output current is increased, leading to lower conversion efficiency at very high currents. A lower conversion efficiency in the submodule MPPTs will lead to lower string power, which can be detected by the global MPPTs algorithm if the output current is increased too much. It should be noted that this effect (decrease in output power by reduced conversion efficiency) is much less pronounced than the relatively sharp drop-off in power observed in a regular PV panel when it operates away from the MPP. The distributed MPPT thus have the effect of significantly "flattening" the power versus voltage (or current) characteristics of the system. The advantage of this is that the central inverter can operate at many different voltage and current levels (while drawing near maximum power from the system). There is, however, a risk that the central inverter may not be able to detect the small changes in power associated with the change in submodule MPPT efficiency, and may continuously wander across a wide current and voltage range as it searches for the global MPPT.

In the experimental measurements of Section V, we will see the results of a control mechanism that makes use of the 1-bit feedback global MPPT algorithm. The flattening effect of the distributed MPPTs will also be observed and enables us to quantify the resolution required to implement the communicationless global MPPT algorithm in practice. It should be noted that both of these control methods still require both local *and* global MPPT algorithms, but the level of communication between the central and local converters differs between the two approaches.

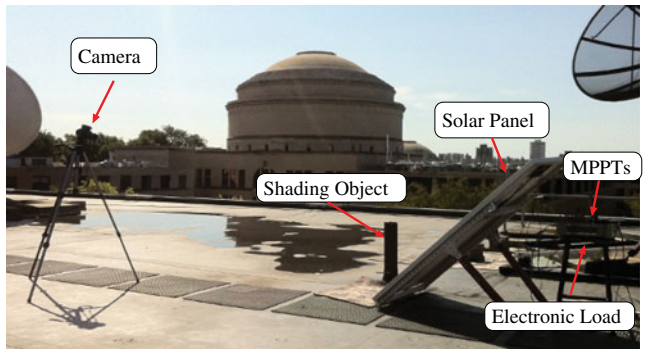

Fig. 6. Annotated photograph of the field experiment setup.

V. Field Measurement Experimental Results

In order to fully evaluate the distributed MPPT system in a real setting, we chose to perform outdoor field experiments under a variety of conditions. A PV panel (the STP175S-24/Ab01 72-cell monocrystalline Si panel from Suntech) was mounted in a south-facing direction together with test equipment on a flat roof of a building on the MIT campus. The camera was used to produce time-lapse photos of the shading pattern of the panel. The photos were synchronized with the output power measurement, providing a visual check to discern shading patterns related to panel *I–V* characteristics. Fig. 6 shows an annotated photograph

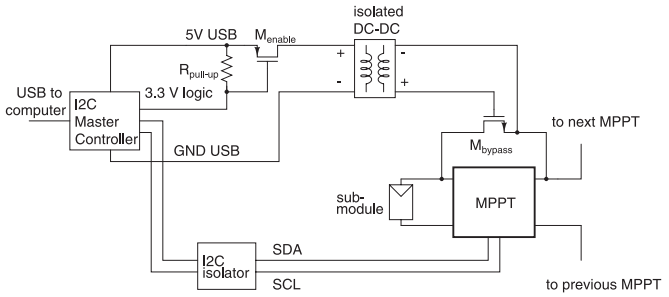

Fig. 7. Schematic drawing of the MPPT bypass circuit which is powered through the USB port and controlled by a general purpose pin on the I2C host adapter.

of the field setup. The distributed MPPTs were connected across each submodule (in parallel with the existing junction diodes, as shown in Fig. 2), and their output is connected to an electronic load (HP6060B). The electronic load was controlled through the GPIB interface by a small netbook computer that recorded all data.

To effectively characterize the performance benefit of the submodule distributed power electronics compared to a conventional solar panel, a low on-state resistance bypass MOSFET (PSMN8R5-60YS by NXP) was used, such that the system could be alternated between employing distributed MPPT (MPPTs on, bypass MOSFET OFF), and conventional operation (MPPTs OFF, bypass MOSFET ON). The bypass MOSFET was connected as shown in Fig. 7, where it can be turned ON or OFF by an isolated dc–dc converter, which is in turn controlled by an enable/disable PMOS driven by a general purpose I/O pin on the USB-connected I2C controller (the Aardvark I2C Host Adapter from Total Phase).

The host adapter provides bidirectional translation of the commands from the USB port to the I2C bus. Custom control software was written in Python to communicate with each MPPT, execute the tracking algorithms, and store data with information about operating voltage, current, and duty cycle of each converter for tracking analysis.

Fig. 8 shows an annotated photograph of the circuit board where the bypass circuit, I2C isolation components, and the MPPTs were mounted, together with connectors. Although each circuit board has room for four MPPTs, only three were employed in our experiments, since our solar panel has three bypass diodes.

A. Static Performance Evaluation

Our first experiment was to evaluate the relative performance improvement offered by the distributed MPPT during a static submodule mismatch scenario. In this case, we performed measurements with and without distributed MPPT for a panel where a single cell experienced various degrees of shading (as shown in Fig. 9). This scenario is representative of static mismatch caused by, for example, dirt accumulation, bird droppings, a damaged cell, or a severe local degradation of the panel encapsulant.

Shown in Fig. 10 is a plot of measured panel output power versus load current when a single cell in the panel is shaded by 50% (as per Fig. 10, under constant outdoor insolation (i.e., a short measurement on a cloud-free day). The solid blue line represents the measurement when the panel was connected directly to the electronic load, without distributed MPPTs. In this case, the electronic load was first connected to each individual submodule to generate a plot of power versus output current. It can be clearly seen that submodule 3 has a lower maximum output current (and hence power) due to the single shaded cell.

Furthermore, from the plot showing the full panel power without distributed MPPT, two maximum power points can be seen. This is due to the bypass diode connected to submodule 3 conducting when the electronic load is drawing more current than the maximum current available from submodule 3. In this case, it can be seen that the global MPP is the case where the bypass diode is not conducting, whereas the other point is a local MPP. Situations like this present problems for the MPPT algorithms in both centralized inverters and microinverters, as they can easily get stuck on the local MPP. Table III provides the MPPT tracking parameters used for this and all subsequent MPPT tests.

The green circles in Fig. 10 represent discrete data points collected with the distributed MPPT converters enabled, for a variety of output currents (stepped by the electronic load). In this measurement, the electronic load stepped the output current to the indicated values with enough time (a few seconds) between steps to ensure that the distributed MPPTs reached their steady-state points after each step. For this shading scenario (a single cell shaded by 50%), a 24% increase in achievable power output can be observed. The increase in power output is of course dependent on the particular shading pattern (we have measured instances of more than 30% increase in output power for certain shading patterns). Furthermore, the panel with integrated submodule MPPTs produces close to its maximum power across a broad range of output currents. In a complete system with a central inverter, this characteristic would enable the inverter to extract maximum power over a wide voltage and current range, rather than the single point associated with a conventional PV system.

It should be noted that in the shading scenario shown in Fig. 10, the distributed MPPT system actually produces an output voltage that is *higher* than what a conventional system would produce, despite the use of synchronous buck converters. In a conventional system, shaded sections are entirely bypassed, thereby reducing the output voltage of the system. In our proposed system, even the weak submodules are able to contribute whatever voltage they can to the output, thereby often-time increasing the output voltage compared to a conventional PV module. DMPPT systems employing buck converters are often erroneously believed to always produce a lower output voltage, but as shown in Fig. 10, this is not always the case. The system must certainly be designed with sufficient voltage headroom to ensure operation across the expected operation range, but in this regard, our system is no different than conventional PV installations which must do the same to account for any bypass diodes conducting due to partial shading.

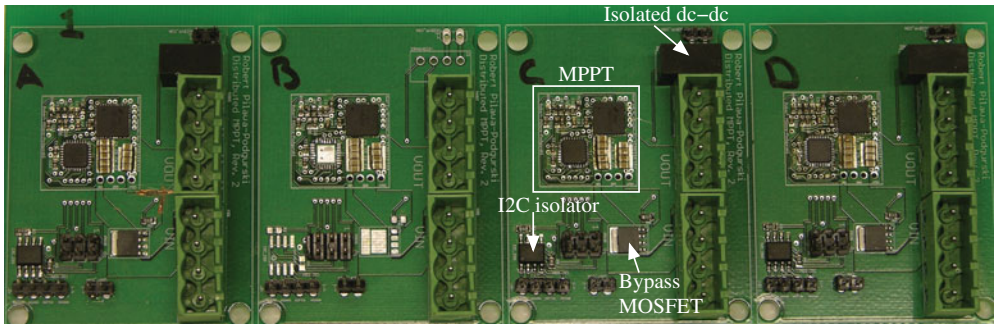

Fig. 8. Annotated photograph of the experimental prototype converters with isolated communication. The bypass MOSFET (powered by the isolated dc–dc converter) enables the MPPT to be bypassed entirely (for evaluation purposes).

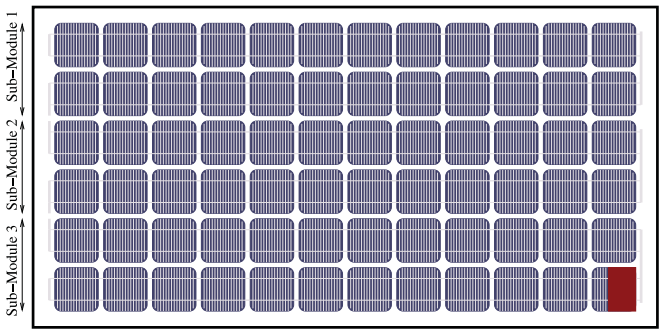

Fig. 9. Drawing of the solar panel illustrating the physical location of the three submodules that are accessible through the junction box (corresponding to the electrical wiring schematic shown in Fig. 2). The bottom right cell in submodule 3 is partially shaded in this experiment. The solar panel used in this experiment was the STP175S-24/Ab01 72-cell monocrystalline Si panel from Suntech.

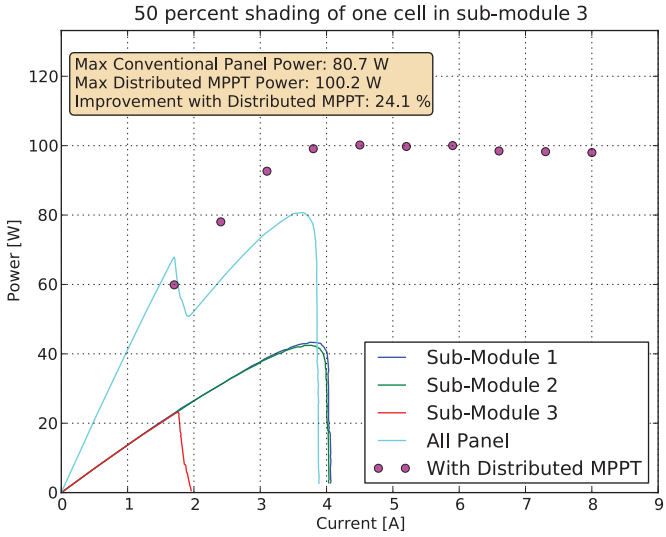

Fig. 10. Plot of power versus current with and without distributed MPPT, for 50% shading of one cell in submodule 3. A power increase of 24% is observed by the use of the submodule MPPTs. These data were taken at MIT on October 6, 2011, which was a very sunny day with no cloud coverage.

We have performed a number of measurements on different static scenarios, details of which can be found in [10]. Table IV summarizes these results, where the relative improvement of the distributed MPPT architecture can be clearly seen. For a perfectly matched panel with no shading throughout the day, however, our proposed system would not be beneficial, as seen from the decrease in output power when employing the distributed MPPT for 0% shading of a single cell. This should come as no surprise, as any added power electronics incur some loss, and if there is no inherent mismatch in the panel, there is nothing to be gained from employing additional MPPTs. It should be pointed out, however, that it is fairly trivial to implement a bypass mode in the MPPTs themselves, such that during times of no shading the MPPTs are bypassed altogether and thus are not contributing any loss. This bypass mode can be implemented in firmware only (turning the top MOSFET ON permanently, with some additional conduction loss in the switch and inductor), or with one additional bypass MOSFET with low on-state resistance (this approach will give the lowest loss in no-shading situations).

TABLE IV
STATIC SHADING PERFORMANCE

Shading of single cell	Panel power without sub-module MPPT	Panel power with sub-module MPPT	Change
75 %	75.2 W	83.5 W	+11.0%
50 %	80.7 W	100.2 W	+24.1%
25 %	103.4 W	115.1 W	+11.3%
0 %	135.5 W	132.4 W	-2.3 %

B. Dynamic Performance Evaluation

To evaluate the performance of the subpanel distributed MPPT architecture under dynamic partial shading conditions, we performed the following field experiment under practical real-world conditions.

The panel was placed near a metal chimney (visible in Fig. 6), so that only a small number of cells were shaded, as illustrated in Fig. 11. As the sun moves throughout the day, the location of the shadow on the panel moves as well, covering different sections of the panel to varying degrees. This situation is very similar to what would happen in residential installations, where chimneys, power lines, trees, antennas, and other structures block parts of the panel throughout the day.

The system was set up such that approximately every minute it would switch between bypassing the distributed MPPTs and connecting them to the panel. When the MPPTs are bypassed (i.e., the panel is configured just like a conventional panel), the

Fig. 11. Photograph illustrating the shading (owing to a protruding pipe) that moves across the panel for the dynamic performance experiment.

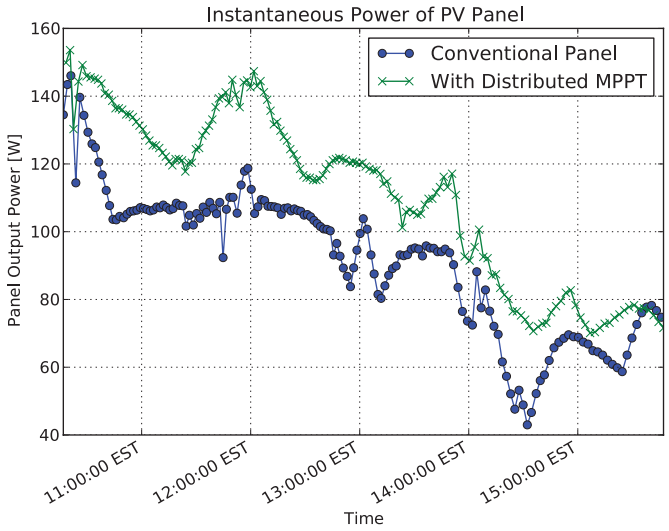

Fig. 12. Instantaneous measured power versus time for a sunny day (October 6, 2011) for a conventional panel, as well as with the distributed MPPT employed, for the test setup illustrated in Fig. 6. Up to a 30% increase in captured power is observed.

electronic load performs a full *I–V* sweep of the panel, and the highest power is recorded. When the MPPTs are connected, the electronic load starts at a current (6 A) that is higher than the panel short-circuit current (5.2 A), and waits for the MPPT outputs to reach steady state (a few seconds). It then decreases the current, at each time waiting for the MPPTs to settle again. It continues to decrease the current until one of the MPPTs (the one connected to the strongest submodule) reaches its maximum allowed duty cycle (0.99). At this time, any further decreases in panel output current will mean that at least one of the MPPTs is not operating at the submodule MPP, so the sweep is stopped, and the highest output power is recorded. This effectively reflects operation with the 1-bit feedback global MPPT algorithm described in Section IV.

Shown in Fig. 12 is a plot of panel output power versus time, with and without the distributed MPPT electronics active, as discussed earlier. These measurements were taken on a very sunny day (October 6, 2011) at the times indicated in the plot.

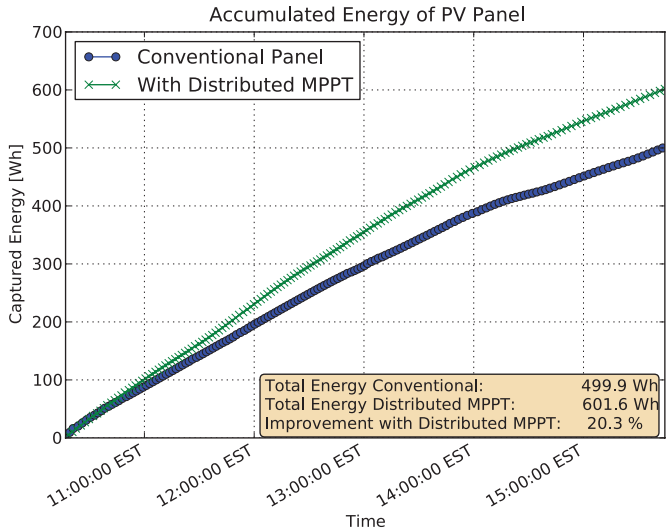

Fig. 13. Accumulated energy versus time for a sunny day (October 6, 2011) for a conventional panel, as well as with the distributed MPPT employed. The distributed MPPT system collects more than 20% additional energy over a conventional panel.

It can be seen that at all times during the measurement period, the distributed MPPT system generated more power from the panel than what a conventional panel would generate, thanks to the mitigation of submodule current mismatch owing to partial shading.

Shown in Fig. 13 is the accumulated energy extracted from the panel during the measurement time, and it shows that the distributed MPPT system collected over 20% more energy over the course of this experiment than what a conventional panel would achieve.

VI. Performance Comparison

The previous section illustrates the improvements in overall power and energy capture that can be realized with the use of the submodule MPPT architecture and the hardware implemented in this study. In solar PV applications, which are very cost sensitive, it is illustrative to perform a cost analysis to quantify the cost-benefit tradeoff of this increase in power. A small increase in output power that comes at a large added system cost is clearly not worthwhile, and in this section, we provide a quantitative analysis of this tradeoff, based on the empirical data captured in our experiment.

Shown in Table V is a comparative chart of our work, previous academic work, as well as two selected commercial solutions. The topology, cost, power density, efficiency, and an FOM (discussed below) are listed. For the academic work, we have attempted to estimate the complete converter cost from published results[3] (the commercial prices are estimates from reported retail prices) and adjusted the efficiencies so that they each include all control and gate driver losses for a fair comparison. It should be noted that aside from the work presented here, none of the other

[3]Note that the cost presented in [6] does not include the cost of the microcontroller, gate driver, auxiliary power supply, and many other components. They are added into the cost used here to provide a fair comparison.

TABLE V
DC–DC OPTIMIZER PERFORMANCE COMPARISON

Work	[6]	[5]	[17]	National	Azuray	This work
Type	Academic	Academic	Academic	Commercial	Commercial	Academic
Topology	Buck-Boost	Boost	Buck-Boost	Unknown	Unknown	Buck
Sub-Module Tracking	No	No	No	No	No	Yes
Volume [cm^3]	255 cm^3	unknown (big)	850 cm^3	680 cm^3	740 cm^3	12 cm^3
Cost	$27	unknown (high)	$65	$150	$90	$12.80
Power [W]	85 W	60 W	100 W	230 W	300 W	200 W
Cost/Power [$/W]	0.32 $/W	high	0.65 $/W	0.65 $/W	0.3 $/W	0.064 $/W
Efficiency [%]	95%	93%	95%	98.5%	97.6%	98.2%
FOM [$/(added W)]	7.06 $/W		14.44 $/W	7.81 $/W	4.07 $/W	0.50 $/W

solutions provide submodule tracking and thus only address mismatch at the panel level. As was shown in the experimental section, submodule mismatch can contribute to significant energy loss (up to 20%), which cannot be mitigated by the other solutions. We find that both in terms of efficiency and cost, our solution compares favorably to previously published work in the field, while also offering a significant increase in overall energy capture during partial shading conditions.

A. FOM

The merits of distributed MPPT in any solar PV system are entirely dependent on the particular installation. Some installations may benefit greatly from added power electronics, whereas others may see no improvement in overall energy capture (e.g., perfectly matched panels on a completely flat surface with no external objects that can cause shading). Due to the very site-specific circumstances, it is therefore difficult to quantify exactly how much a typical residential installation may benefit from our approach. It is, however, possible to quantify the relative merits of the power electronic solution itself, compared to other similar solutions. This is done in Table V, where we have introduced an FOM that aims to capture some of the cost/benefit tradeoff with this approach. It should be pointed out that this FOM is a crude estimate of the relative performance between different solutions, and it should not be used as an absolute metric to judge whether distributed MPPT will pay off or not.

The FOM attempts to capture the incremental cost for the added average power to the PV system (given as $/Watt). It calculates the expected additional average power captured by the system (accounting for the electrical conversion losses of the MPPTs in each case), for a given nominal power increase factor α. This increase factor represents the fractional increase in average output power that can be expected with the distributed MPPT system and, as such, is highly installation dependent. For our analysis, an α of 0.1 is chosen for per-panel MPPT and 0.15 for submodule MPPT (this is a modest 5% increase for submodule MPPT compared to per-panel MPPT, keeping in mind that we experimentally measured between a 10% and 20% increase in captured energy for the submodule case versus regular panel-based MPPT in our field experiments). The FOM is given by

$$\text{FOM} = \frac{\text{cost}}{\langle P_{\text{added}} \rangle} \tag{3}$$

where P_{added} is the *additional* power captured owing to the power electronics

$$\langle P_{\text{added}} \rangle = \eta_{\text{MPPT}} P_{\text{rated}} (1 + \alpha) - P_{\text{rated}} \tag{4}$$

and η_{MPPT} is the electrical conversion efficiency of the MPPTs, and P_{rated} is the rated power of the MPPT. The FOM should be compared to the typical installed cost of solar PV systems, which was estimated to be around $6/W in 2010 [18], but is rapidly decreasing. In order for the distributed MPPT system to be cost effective, the FOM must be below the installed cost of the PV system, for a given installation. We see that for our assumptions of a 10% and 15% total improvement in average power due to module and submodule tracking, respectively, the cost benefit of many of the solutions of Table V are marginal. As the installed cost of solar PV continues to decrease, even further price pressure on the power electronics is expected. In light of this, our calculated FOM of 0.50 $/W makes our solution cost competitive today, and for some time in the future.

It should be pointed out again that the FOM is highly dependent on the parameter α, which attempts to quantify the performance improvements offered by distributed MPPT. It is certainly possible to better quantify this improvement with a more detailed FOM that models the length of shading (in time), additional panels, and weather data. Our attempt here was merely to elucidate some of the tradeoffs in terms of cost and performance, with rough estimates guided by our empirical data.

Finally, we should mention that the FOM described here only captures the monetary value associated with increased energy capture. Distributed power electronics in solar PV installations can provide additional benefits in terms of per-panel (or submodule) diagnostics and data capture, enabling the user to quickly isolate and replace malfunctioning panels. Distributed power electronics also enables added protection with its ability to completely turn off the panel output current, something which is not possible with a simple series string architecture. It is expected that these additional services will receive more attention in the future and may become as important as the increased energy capture in choosing a system architecture.

VII. CONCLUSION

We have presented a submodule distributed MPPT architecture for solar PV applications, which enables more energy to be extracted from the system. By employing low-voltage synchronous buck converters connected across each submodule of the panel, a high-frequency, very high-efficiency power stage

can be used. The power electronics can then be miniaturized to the point where they fit into the existing junction box, thereby greatly reducing cost. We have presented a hardware prototype for use in submodule tracking of a PV panel, and discuss local and global control techniques to maximize the overall energy capture of the system. We measure up to a 20% improvement in overall energy capture compared to per-panel MPPT implementation, using field experiments with a partial shading obstacle, and perform static mismatch measurements that further validate the performance of the system. Finally, we compare our implementation to other state-of-the-art commercial and academic solutions, and find that the proposed solution offers attractive benefits in terms of efficiency and cost, both of which are critical in PV systems.

REFERENCES

[1] "Trends in photovoltaic applications. Survey report of selected IEA countries between 1992 and 2006," Int. Energy Agency Photovoltaic Power Syst., Paris, France, Tech. Rep. IEA-PVPS T1-16:2007, 2007 [Online]. Available at www.iea-pvps.org

[2] S. Kjaer, J. Pedersen, and F. Blaabjerg, "A review of single-phase grid-connected inverters for photovoltaic modules," *IEEE Trans. Ind. Appl.*, vol. 41, no. 5, pp. 1292–1306, 2005.

[3] J. Myrzik and M. Calais, "String and module integrated inverters for single-phase grid connected photovoltaic systems: A review," in *Proc. IEEE Bologna Power Tech.*, Jun. 2003, p. 8.

[4] T. Shimizu, M. Hirakata, T. Kamezawa, and H. Watanabe, "Generation control circuit for photovoltaic modules," *IEEE Trans. Power Electron.*, vol. 16, no. 3, pp. 293–300, May 2001.

[5] G. R. Walker and P. C. Sernia, "Cascaded dc–dc converter connection of photovoltaic modules," *IEEE Trans. Power Electron.*, vol. 19, no. 4, pp. 1130–1139, 2004.

[6] L. Linares, R. W. Erickson, S. MacAlpine, and M. Brandemuehl, "Improved energy capture in series string photovoltaics via smart distributed power electronics," in *Proc. 24th Annu. IEEE Appl. Power Electron. Conf. Expo.*, Feb. 2009, pp. 904–910.

[7] J. Stauth, M. Seeman, and K. Kesarwani, "A high-voltage CMOS IC and embedded system for distributed photovoltaic energy optimization with over 99% effective conversion efficiency and insertion loss below 0.1%," in *Proc. IEEE Int. Solid-State Circuits Conf.*, Feb. 2012, pp. 100–102.

[8] G. Adinolfi, N. Femia, G. Petrone, G. Spagnuolo, and M. Vitelli, "Design of dc/dc converters for DMPPT PV applications based on the concept of energetic efficiency," *J. Solar Energy Eng.*, vol. 132, pp. 021005-1–021005-10, 2010.

[9] R. Alonso, E. Roman, A. Sanz, V. E. M. Santos, and P. Ibanez, "Analysis of inverter-voltage influence on distributed MPPT architecture performance," vol. 59, no. 10, pp. 3900–3907, 2012.

[10] R. C. N. Pilawa-Podgurski, "Architectures and circuits for low-voltage energy conversion and applications in renewable energy and power management" Ph.D. dissertation, Dept. Electr. Eng. Comput. Sci. Massachusetts Inst. Technol., Cambridge, 2012.

[11] R. C. N. Pilawa-Podgurski, N. A. Pallo, W. R. Chan, D. J. Perreault, and I. L. Celanovic, "Low-power maximum power point tracker with digital control for thermophotovoltaic generators," in *Proc. 25th Annu. IEEE Appl. Power Electron. Conf. Expo.*, Feb. 2010, pp. 961–967.

[12] N. Femia, G. Lisi, G. Petrone, G. Spagnuolo, and M. Vitelli, "Distributed maximum power point tracking of photovoltaic arrays: Novel approach and system analysis," *IEEE Trans. Ind. Electron.*, vol. 55, no. 7, pp. 2610–2621, 2008.

[13] T. Shimizu, O. Hashimoto, and G. Kimura, "A novel high-performance utility-interactive photovoltaic inverter system," *IEEE Trans. Power Electron.*, vol. 18, no. 2, pp. 704–711, 2003.

[14] G. Petrone, C. A. Ramos-Paja, G. Spagnuolo, and M. Vitelli, "Granular control of photovoltaic arrays by means of a multi-output maximum power point tracking algorithm," *Progr. Photovoltaics: Res. Appl.*, 2012. doi: 10.1002/pip.2179.

[15] D. Perreault, R. L. Selders, Jr., and J. Kassakian, "Frequency-based current-sharing techniques for paralleled power converters," *IEEE Trans. Power. Electron.*, vol. 13, no. 4, pp. 626–634, 1998.

[16] D. Perreault, K. Sato, R. L. Selders, Jr., and J. Kassakian, "Switching-ripple-based current sharing for paralleled power converters," *IEEE Trans. Circuits Syst.—Part I: Fundamental Theory Appl.*, vol. 46, no. 10, pp. 1264–1274, 1999.

[17] E. Roman, R. Alonso, P. Ibanez, S. Elorduizapatarietxe, and D. Goitia, "Intelligent PV module for grid-connected PV systems," *IEEE Trans. Ind. Electron.*, vol. 53, no. 4, pp. 1066–1073, Jun. 2006.

[18] G. Barbose, N. Darghouth, R. Wiser, and J. Seel, "Tracking the sun IV: A historical summary of the installed cost of photovoltaics in the United States from 1998 to 2010," Lawrence Berkeley Nat. Lab., Berkeley, CA, Rep. LBNL-5047E, 2011

Robert C. N. Pilawa-Podgurski (S'06–M'11) was born in Hedemora, Sweden. He received dual B.S. degrees in physics, electrical engineering, and computer science in 2005, the M.Eng. degree in electrical engineering and computer science in 2007, and the Ph.D. degree in electrical engineering in 2012, all from the Massachusetts Institute of Technology, Cambridge.

He is currently an Assistant Professor in the Department of Electrical and Computer Engineering, University of Illinois, Urbana-Champaign, Urbana, and is affiliated with the Power and Energy Systems group. He performs research in the area of power electronics. His research interests include renewable energy applications, energy harvesting, CMOS power management, and advanced control of power converters.

David J. Perreault (S'91–M'97–SM'06) received the B.S. degree from Boston University, Boston, MA, and the S.M. and Ph.D. degrees from the Massachusetts Institute of Technology (MIT), Cambridge.

In 1997, he joined the MIT Laboratory for Electromagnetic and Electronic Systems as a Postdoctoral Associate, and became a Research Scientist in the laboratory in 1999. In 2001, he joined the Department of Electrical Engineering and Computer Science, MIT, where he is currently a Professor of Electrical Engineering. His research interests include design, manufacturing, and control techniques for power electronic systems and components, and in their use in a wide range of applications.

Dr. Perreault received the Richard M. Bass Outstanding Young Power Electronics Engineer Award from the IEEE Power Electronics Society, an ONR Young Investigator Award, and the SAE Ralph R. Teetor Educational Award. He is a co-author of four IEEE prize papers.